

# Carbon Structure of Coal from the CP/MAS $^{13}\text{C}$ NMR Spectra: Effect of Contact Time and Potential Quantitative Modification

Tong Lv, Mengxiang Fang,\* Xi Zeng, Jiqing Yan, Yu Huang, Jianmeng Cen, and Qinhui Wang



Cite This: *Energy Fuels* 2024, 38, 3740–3754



Read Online

ACCESS |



Metrics & More

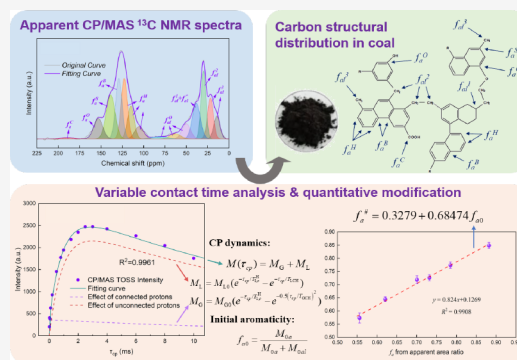


Article Recommendations



Supporting Information

**ABSTRACT:** Carbon structures are important for converting coal into chemical products and carbon materials. Solid-state  $^{13}\text{C}$  nuclear magnetic resonance (NMR) spectroscopy is a powerful approach for determining the structural characteristics of carbon in coal. However, there is much controversy regarding the quantitative reliability of typical cross-polarization magic angle spinning (CP/MAS)  $^{13}\text{C}$  NMR experiments of coal. This study systematically investigated the effect of one of the important factors, CP contact time, using six different coal types with  $V_{\text{daf}}$  values ranging from 6% to 44%. A series of experimental results at variable contact times from 0.01 to 10 ms indicated that aromatic and aliphatic carbons undergo polarization transfer at different rates, and the nonprotonated carbon of aromatic groups polarized 2–3 times more slowly than that of aliphatic groups. It is challenging for a single CP/MAS  $^{13}\text{C}$  NMR experiment with coal to ensure that each type of carbon is sufficiently polarized before the signal decay of the proton spin–lattice relaxation. As a potential quantitative indicator, the initial magnetization intensity independent of contact time was obtained using a classical five-parameter model for CP dynamics, and the initial aromaticity was further calculated. A linear correlation between the apparent and initial aromaticity was introduced into a calibration method of model compounds to refine the effect of contact time. The modified carbon structural parameters of the coal samples showed better agreement in terms of the H/C atomic ratio, Fourier transform infrared spectroscopy, and empirical aromaticity formulas. These results will help to provide a convenient reference for the quantitative analysis of the carbon structure in coal.



## 1. INTRODUCTION

Coal is an essential fossil fuel and a chemical resource with a high carbon content and heterogeneous structures. With increasing requirements for carbon neutrality, coal utilization is gradually changing from traditional combustion for power generation to clean and efficient multilevel development.<sup>1–5</sup> The chemical structure of coal determines its reactivity during the conversion process; in particular, the carbon skeletal structure dominates the evolution of the main organic products.<sup>6–9</sup> Solid-state  $^{13}\text{C}$  nuclear magnetic resonance (NMR) spectroscopy is a powerful nondestructive approach for determining the structural characteristics of various carbonaceous materials. The development of cross-polarization (CP) and magic angle spinning (MAS) technologies in the 1970s<sup>10,11</sup> enabled the convenient and effective application of  $^{13}\text{C}$  NMR spectroscopy in solid fuels with complex components, such as coal. In the CP experiments, the magnetization signal of the  $^{13}\text{C}$  nucleus was enhanced by the polarization transfer from protons to carbon, and the MAS conditions eliminated the effect of chemical shift anisotropy for solid substances. The rapid rotating sideband of the aromatic structures in coal samples could be reduced by the total suppression of spinning sidebands (TOSS) sequence.<sup>12</sup> Consequently, solid-state  $^{13}\text{C}$  NMR spectra of coal with high

sensitivity and resolution were obtained by combining the CP, MAS, and TOSS technologies.

It is generally believed that the organic macromolecules of coal consist of many condensed aromatic rings interconnected by various nonaromatic bridge bonds and may be attached to several alkyl side chains and functional groups.<sup>13–15</sup> The  $^{13}\text{C}$  NMR spectra reflected the carbon distribution in terms of the aromatic and aliphatic structures, and some parameters could be deduced to describe the carbon skeleton in the coal. The most representative structural parameters were first proposed by Solum et al.,<sup>16</sup> and most studies in subsequent decades have continued or extended their methods. One of the most important parameters, aromaticity ( $f_a$ ), is a good measurement for evaluating the carbon maturity among different coal ranks.<sup>17,18</sup> Carbon structures derived from  $^{13}\text{C}$  NMR facilitate the development of modeling methods for coal molecules and their conversion behaviors, such as chemical percolation

Received: November 28, 2023

Revised: January 18, 2024

Accepted: January 22, 2024

Published: February 8, 2024



Table 1. Proximate and Ultimate Analyses of Raw and Acid-Washed Coal Samples

sample	proximate analysis (wt %) <sup>a</sup>				ultimate analysis (wt %) <sub>daf</sub>				
	M <sub>ad</sub>	A <sub>d</sub>	V <sub>daf</sub>	FC <sub>daf</sub>	C	H	N	S	O <sup>b</sup>
HCG	1.84	9.63	40.27	59.73	82.83	5.64	2.04	0.91	8.58
HCG-AW <sup>c</sup>	2.40	0.94	44.50	55.50	84.51	5.68	1.88	0.87	7.06
XG	1.89	10.14	34.52	65.48	82.83	5.26	1.55	0.99	9.37
XG-AW	3.39	0.86	32.05	67.95	85.92	5.11	1.49	1.02	6.46
JL	1.92	9.90	28.95	71.05	88.28	4.96	1.60	2.24	2.93
JL-AW	1.83	0.50	26.70	73.30	89.72	4.99	1.41	1.61	2.26
LL	0.89	6.98	19.64	80.36	87.58	4.53	1.37	3.08	3.44
LL-AW	1.25	0.42	18.13	81.87	90.79	4.78	1.24	2.62	0.57
MHL	1.10	12.19	14.34	85.66	88.16	4.15	1.24	2.41	4.04
MHL-AW	1.75	0.58	12.65	87.35	91.94	4.21	1.11	2.05	0.69
PDS	2.42	13.22	7.88	92.12	93.05	3.44	1.32	0.69	1.51
PDS-AW	3.84	0.40	6.61	93.39	94.16	3.69	1.16	0.62	0.36

<sup>a</sup>ad, air-dry basis; d, dry basis; daf, dry ash-free basis. <sup>b</sup>By difference. <sup>c</sup>AW, acid washed.

devolatilization (CPD)<sup>19,20</sup> and FLASHCHAIN<sup>21–23</sup> pyrolysis models. Moreover, the solid-state CP/MAS <sup>13</sup>C NMR spectroscopy has also been widely applied to analyze the carbon structure of coal-based products during liquefaction and hydrothermal processes,<sup>24–28</sup> which can not only indicate the reaction mechanism but also develop models and correlations to predict conversion results.

The magnetization intensity in a <sup>13</sup>C NMR spectrum is related to the quantity of different types of carbon atoms, and therefore peak-fitting or interval integration from a single CP/MAS <sup>13</sup>C NMR spectrum has been utilized to determine the carbon distribution in many studies.<sup>29–31</sup> However, there has been much debate on the quantitative reliability of the CP/MAS experiments when using coals with complex and heterogeneous structures as samples.<sup>12,32–34</sup> Some studies<sup>32,35,36</sup> have reported that the apparent intensity of <sup>13</sup>C NMR spectra is merely qualitative, and the derived structural parameters deviate from other analytical approaches to some extent. Values for the carbon aromaticity of coals obtained from the CP experiments are generally lower than those from the Bloch-decay experiments.<sup>33,34</sup> In the CP/MAS <sup>13</sup>C NMR experiments, aromatic and aliphatic carbons have different cross-polarization efficiencies; thus, a single spectrum at insufficient contact time may not entirely represent the magnetization of all carbon types.<sup>33,36</sup> Furthermore, even for aliphatic carbon alone, the rate of polarization is affected by the number of attached protons and the distance from the surrounding protons.<sup>34</sup> In order to make the CP/MAS <sup>13</sup>C NMR spectra of coal as quantitative as possible, several methods have been developed to reduce the deviations through the design of novel experiments or standard calibration curves. Yang et al.<sup>36</sup> investigated variable contact time CP/MAS <sup>13</sup>C NMR spectra to correct the underestimation of the aromatic carbon parameters. Li et al.<sup>35</sup> directly adopted the H/C atomic ratio from the ultimate analyses to redistribute the percentages of aromatic and aliphatic carbons. Guo et al.<sup>37</sup> corrected the carbon parameters using the Solomon equation and validated the equation using the Boltzmann–Monte Carlo-percolation (BMCP) model, which predicts the pyrolysis behavior of coals. Chen et al.<sup>32</sup> conducted the CP/MAS <sup>13</sup>C NMR experiments using model coal compounds and fitted a nonlinear regression equation to calibrate the apparent carbon fraction, which was initially validated by Bian et al.<sup>38</sup> when constructing a molecular model of medium-rank coal. Nevertheless, to date, there are still

numerous studies on coal molecular modeling without any modifications when using the results from the peak fitting of the CP/MAS <sup>13</sup>C NMR spectra.<sup>39–41</sup> Few studies have systematically reported the influencing mechanism and a comparison between these corrections. In conclusion, more efforts are required to optimize or verify the analytical methods for the CP/MAS <sup>13</sup>C NMR spectroscopy of coal.

To investigate the difference in polarization rates of aliphatic and aromatic carbons and analyze the possible reasons for the controversy of the apparent parameters from the <sup>13</sup>C NMR spectra of coal, this study conducted a series of variable contact time CP experiments using six different coal types with V<sub>daf</sub> ranging from 6% to 44%, and the CP dynamics were analyzed using representative exponential models. The initial magnetization was estimated by extrapolating the integrals to zero contact time, and a linear regression expression was applied to correlate the apparent aromaticity with that independent of time. Furthermore, a modification considering contact time was proposed for improving an existing calibration method on the CP/MAS <sup>13</sup>C NMR spectra of coal, which showed good agreement in terms of the H/C atomic ratio, Fourier transform infrared (FTIR) spectroscopy, and typical empirical aromaticity correlations of coal. These results have the potential to provide a reference for the quantitative application of <sup>13</sup>C NMR spectroscopy in a more convenient way and may contribute to research on the mechanism of coal conversion to chemical products and carbon materials.

## 2. EXPERIMENTAL SECTION

**2.1. Coal Samples.** Six Chinese raw coals with different V<sub>daf</sub> values were selected as samples in this study. The bituminous coals Hecaogou (HCG), Xiegou (XG), Jinliao (JL), Liulin (LL), and Mahuangliang (MHL) were obtained from Shanxi Province, and the anthracite Pingdingshan (PDS) was obtained from Henan Province. These coal samples were crushed and ground to a particle size less than 0.15 mm and dried at 50 °C for 24 h. To avoid damage to the NMR spectrometer caused by magnetic minerals in coal, the pulverized coal samples were acid washed with HCl–HF prior to the experiments.<sup>29,42</sup> Detailed procedures of acid treatment are described in our previous work.<sup>43</sup> The proximate and ultimate analyses of raw and acid-washed coals are presented in Table 1, where the ash contents of all acid-washed coal samples are <1%. According to previous studies<sup>44,45</sup> and our pre-experimental results (as shown in Figure S1 and Table

S1), the deashing process by HCl–HF acid treatment has virtually no effect on the carbon skeleton structures of coal. The following sections in this study will address only acid-washed coals unless otherwise specifically stated.

**2.2..  $^{13}\text{C}$  NMR Spectroscopy.** Solid-state CP/MAS  $^{13}\text{C}$  NMR spectra of the coal samples were obtained using a Bruker AVANCE 400 NMR spectrometer at a frequency of 100.62 MHz for carbon and 400.13 MHz for proton. The magic angle rotation speed was 10 kHz using a 4 mm  $\text{ZrO}_2$  double resonance rotor, and all experiments were performed with the TOSS sequence. The standard CP contact time was 2 ms, with a recycle delay of 4 s and a scan number of 6000. The variable contact time spectra were measured at 16 different contact times ranging from 0.01 to 10 ms with all other conditions constant. Tetramethyl silane was used as an internal standard to calibrate chemical shifts ( $\delta_{\text{TMS}} = 0$  ppm). The integral areas of the main regions in the CP/MAS  $^{13}\text{C}$  NMR spectra were analyzed using MestReNova 12.0 software, and the denoising and baseline corrections of spectra were performed in its default mode. The curve fitting of each spectrum was conducted in the deconvolution mode of PeakFit 4.12 software.

**2.3. FTIR Spectroscopy.** FTIR experiments on the coal samples were conducted by using a Thermo Scientific Nicolet iS20 infrared spectrometer. Approximately 1 mg of the coal sample and 100 mg of dried KBr were added to a mortar and ground thoroughly. The mixture was placed in a sample presser at 20 MPa for 1 min to obtain a sample slice. The slices were secured with a sample holder and placed in an IR spectrometer sample chamber for testing. The spectral range is 4000–400  $\text{cm}^{-1}$  with a resolution of 4.0  $\text{cm}^{-1}$ , and the cumulative number of scans was 32 times for each sample. The baseline correction of the FTIR spectra was performed by using the OMINC 8.2 software, and curve fitting in each region was also conducted by using the PeakFit 4.12 software.

### 3. RESULTS AND DISCUSSION

**3.1. Carbon Classification in  $^{13}\text{C}$  NMR Spectra.** The solid-state CP/MAS  $^{13}\text{C}$  NMR spectra of the six coal samples at the standard CP contact time are shown in Figure 1, where the signal amplitudes are normalized to present the difference in coal ranks more clearly. Two major peaks in the spectra were located at 0–90 and 90–165 ppm, which represent the aliphatic and aromatic carbons in coal, respectively. The region

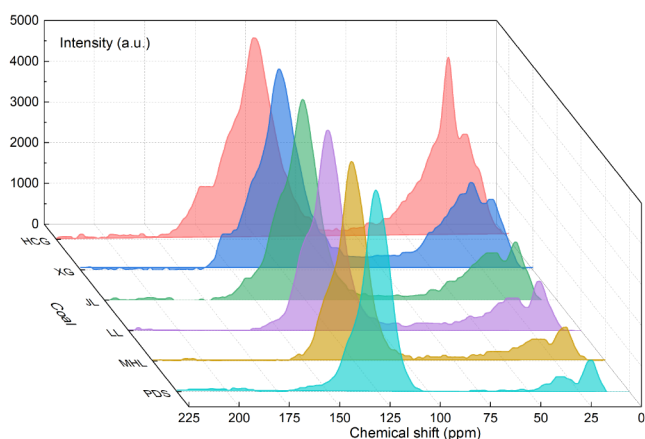


**Figure 1.** Solid-state CP/MAS  $^{13}\text{C}$  NMR spectra of coal samples (at  $\tau_{\text{cp}} = 2$  ms).

greater than 165 ppm corresponds to carbon in the structures containing carbonyl groups, although its intensity was very low for each coal in this study. Figure 2 summarizes the intensity

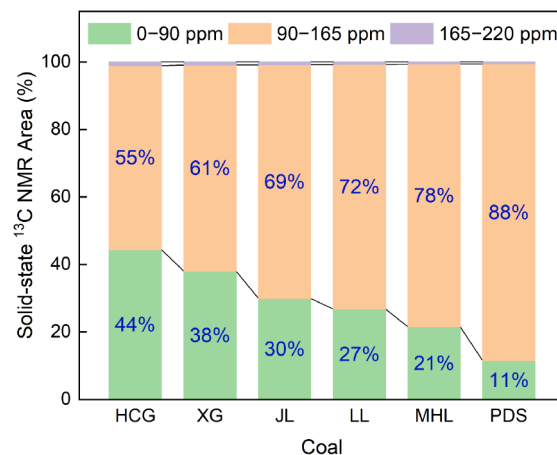


**Figure 2.** Area ratios of coal samples in solid state  $^{13}\text{C}$  NMR spectra.

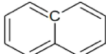
integral area ratios of the three main regions in the  $^{13}\text{C}$  NMR spectra of the coal samples. As the coal rank increases (from 44.5% to 6.6% for  $V_{\text{dar}}$ ), the area of aromatic carbons increases from 55% to 88%, which is consistent with the fact that the higher the coalification, the more stable the coal structure. Most recognized studies<sup>16,46,47</sup> have defined aromaticity ( $f_a$ ) as the carbon fraction with a chemical shift >90 ppm and strict or true aromaticity ( $f_a'$ ) as the fraction excluding the carbonyl group. The former is mainly adopted in the following discussion, and the relationship between them is shown in eq 1. Typically, apparent aromaticity is equal to the integral area ratio of 90–220 ppm in the  $^{13}\text{C}$  NMR spectrum of coal.

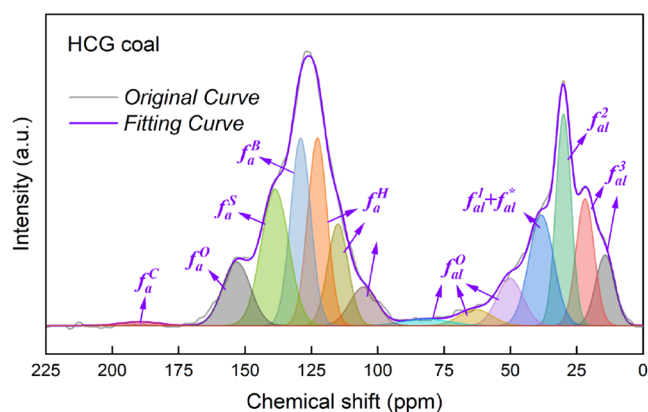
$$f_a' = f_a \times \frac{I_{90-165}}{I_{90-220}} \quad (1)$$

The subdivisions of the aliphatic and aromatic regions are summarized in Table 2 with reference to previous studies.<sup>25,37,38,48,49</sup> The superscripts for the carbon type symbols in this paper also mainly followed previous studies<sup>16,26</sup> with some modifications. For aliphatic carbons, they represent the number of hydrogen atoms attached ( $f_{\text{al}}^3$ ,  $f_{\text{al}}^2$ ,  $f_{\text{al}}^1$ , and  $f_{\text{al}}^*$ ) or the connection to oxygen atoms ( $f_{\text{al}}^{\text{O}}$ ); for aromatic carbons, they denote the type of connecting groups: proton ( $f_a^{\text{H}}$ ), bridgehead carbon ( $f_a^{\text{B}}$ ), alkyl substituent ( $f_a^{\text{S}}$ ), and oxygen ( $f_a^{\text{O}}$ ). Representative peak separation of the CP/MAS  $^{13}\text{C}$  NMR spectrum is shown in Figure 3, taking HCG coal as an example. Detailed results for all coal samples are presented in Figure S2, and their peak information is listed in Table S2, according to the assignments of different chemical shifts. All fitting curves are in excellent agreement with the original spectra ( $R^2 > 0.995$ ). The apparent carbon structural parameters derived from the fitted curves are listed in Table 3. Notably, although the quantitative reliability of the CP/MAS NMR needs further discussion, the qualitative variations are also valuable for the analysis of carbon structural evolution along with coalification.

Aliphatic groups generally play the roles of bridge bonds or side chains in the macromolecular network of coal. As shown in Figure 2, the magnetization intensity of aliphatic carbons at

**Table 2. Assignments of Chemical Shift in the Solid-State  $^{13}\text{C}$  NMR Spectra of Coal Samples**

$\delta$ (ppm)	Carbon structure	Location	Symbols
14–16	Aliphatic methyl	R-CH <sub>3</sub>	
16–22	Aromatic methyl		$f_{al}^3$
22–36	Methylene	-CH <sub>2</sub>	$f_{al}^2$
36–50	Methine, quaternary sp <sup>3</sup> C	-CH, -C	$f_{al}^1, f_{al}^*$
50–90	Oxygen aliphatic carbon	R-O-R	$f_{al}^O$
90–125	Protonated aromatic carbon		$f_a^H$
125–137	Bridgehead aromatic carbon		$f_a^B$
137–148	Aliphatic substituted aromatic carbon		$f_a^S$
148–165	Oxygen aromatic carbon		$f_a^O$
165–220	Carboxyl and carbonyl carbon	-COOH, C=O	$f_a^C$

**Figure 3.** Fitting curves of the  $^{13}\text{C}$  NMR spectra of HCG coal.

the same CP contact time decreases with the coal rank, which indicates the growing carbon skeleton maturity of coal owing to the deoxidation and aromatization reactions during coalification.<sup>50</sup> The peak height of aliphatic carbons depends on methylene for relatively low-rank coals, such as HCG, whereas the methyl groups with chemical shifts of <25 ppm gradually dominate the aliphatic region of the spectra with

decreasing volatile matter in coal. Almost no aliphatic carbon bonded to oxygen was found in the  $^{13}\text{C}$  NMR spectra of PDS anthracite.

Aromatic clusters form the core of the organic structure of coal, and the condensation of aromatic rings usually increases with the deepening of coal metamorphism.<sup>42</sup> The aromatic carbon peaks in Figure 2 gradually sharpen from HCG to PDS, indicating an increasing degree of order for the aromatic structures.<sup>45,51</sup> As can be seen from the apparent parameters in Table 4, the intensity of the protonated aromatic carbon is always the largest regardless of the coal type, and the ratio of bridgehead carbon (a carbon type that occurs only in the fused rings) to total aromatic carbon is positively correlated with the degree of coalification. Similarly, the intensity of the aromatic carbon bonded to oxygen was quite low for high-rank coals. These results also confirmed that the aliphatic and oxygen-containing side chains were removed when the aromatic core underwent polycondensation during coal formation.

**3.2. Variable Contact Time Experiments.** **3.2.1. Effect of CP Contact Time.** The magnetization intensity in solid-state  $^{13}\text{C}$  NMR spectra is a function of the CP contact time, which is an important factor that influences quantitative reliability. Extensive testing experience has demonstrated that there exists an “optimal” contact time ( $\sim 1$ –3 ms) to obtain the CP/MAS  $^{13}\text{C}$  spectra with the highest signal-to-noise ratio.<sup>16,33,52</sup> However, contradictory results under seemingly optimal conditions remain regarding whether carbon magnetization can accurately reflect different carbon concentrations in a single CP/MAS  $^{13}\text{C}$  NMR spectrum of coal. Representative examples from this study are shown in Figure 4. Figure 4a shows that the intensities of aliphatic and aromatic carbons vary differently for HCG coal when contact time ranges from 0.5 to 3 ms. The peak height of aliphatic carbons is higher than that of aromatic carbons at 0.5–1 ms, but a reversal appears at 3 ms. More precisely, the magnetization intensity of aromatic carbons continuously increases, whereas that of aliphatic carbons first increases and then decreases. By contrast, the effect of the contact time on the  $^{13}\text{C}$  NMR spectra is relatively weak for a higher rank of coal (LL), as shown in Figure 4b. It can be even inferred that the apparent intensity distribution is approximately constant under any CP condition if highly mature coal contains almost no aliphatic groups.

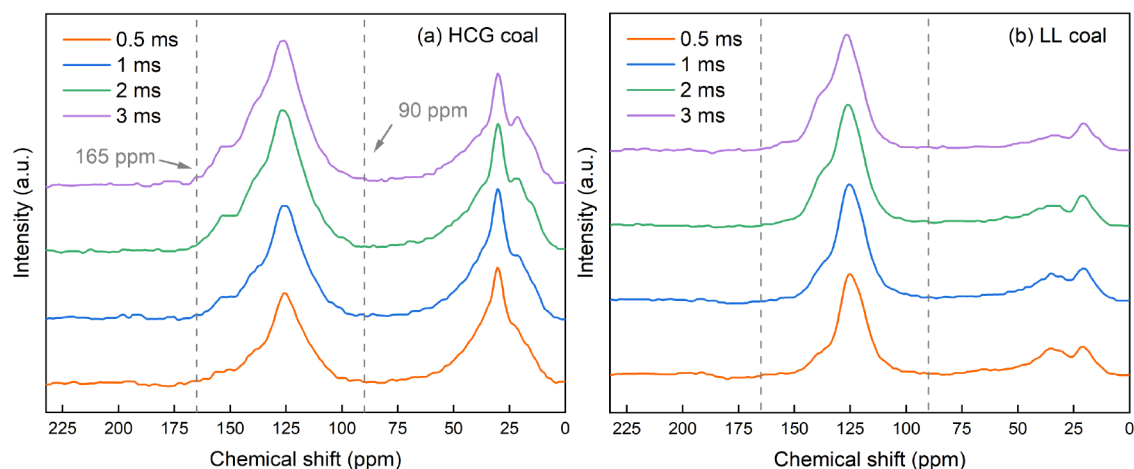
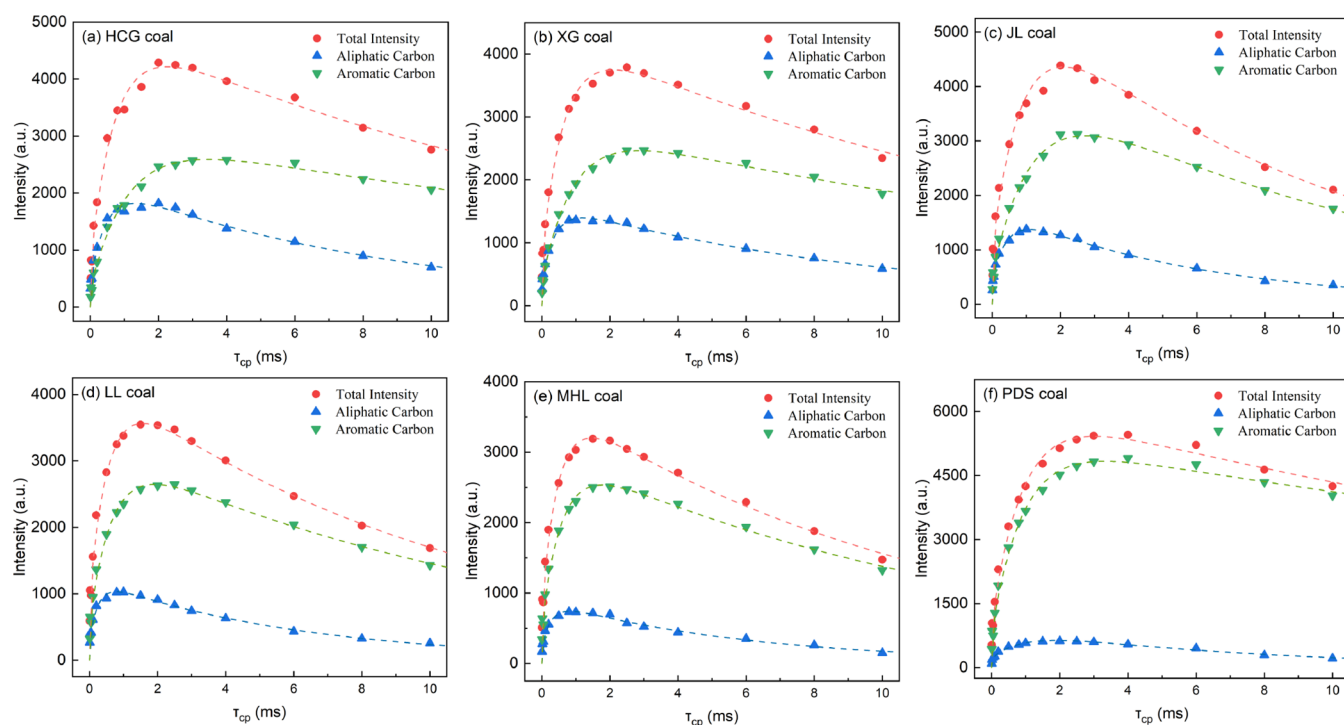
Detailed changes in the magnetization intensity of these coals at a series of contact times are shown in Figure 5. As contact time varies from 0.01 to 10 ms, there is always a tendency for the total signal intensity to increase and then decrease for all samples, with the maximum values occurring at  $\sim 2$  ms. This explains why the single CP/MAS  $^{13}\text{C}$  NMR experiments in many studies<sup>18,35,40,53</sup> were usually performed at a contact time of 2 ms, including the selection of spectra for peak fitting in Section 3.1. However, the contact time

**Table 3. Apparent Carbon Distribution (%) of Coal Samples from the Fitting Curve of the  $^{13}\text{C}$  NMR Spectra**

coal	$f_a$	$f_a'$	$f_a^H$	$f_a^B$	$f_a^S$	$f_a^O$	$f_a^C$	$f_{al}$	$f_{al}^3$	$f_{al}^2$	$f_{al}^1 + f_{al}^*$	$f_{al}^O$
HCG	55.57	54.51	23.07	14.26	11.22	6.04	1.06	44.43	13.33	12.74	10.44	7.93
XG	62.06	61.20	26.62	18.53	10.95	5.22	0.86	37.94	10.61	9.80	7.64	9.89
JL	70.07	69.26	29.67	20.95	12.97	5.79	0.81	29.93	8.42	8.35	6.94	6.21
LL	73.21	72.44	31.10	21.30	14.83	5.42	0.77	26.79	8.41	5.71	4.88	7.79
MHL	78.51	77.87	32.42	26.96	15.15	3.51	0.64	21.49	7.59	5.95	3.20	4.75
PDS	88.24	87.71	36.83	29.90	17.74	3.45	0.53	11.76	6.35	4.65	0.46	0.30

Table 4. Initial Magnetization and Time Constants Calculated by eq 3 for Coal Samples

coal	aliphatic region					aromatic region				
	$M_{G0}$	$M_{L0}$	$T_{GCH}$ ( $\mu$ s)	$T_{LCH}$ ( $\mu$ s)	$T_{1\rho}^H$ (ms)	$M_{G0}$	$M_{L0}$	$T_{GCH}$ ( $\mu$ s)	$T_{LCH}$ ( $\mu$ s)	$T_{1\rho}^H$ (ms)
HCG	414.7	1814.7	6.4	456.1	8.9	308.2	2688.9	8.4	1032.1	30.3
XG	372.3	1261.2	7.2	379.6	10.2	365.1	2598.7	8.5	914.1	20.6
JL	420.9	1351.0	8.3	422.8	6.0	534.2	3995.9	8.6	1178.4	10.5
LL	325.4	903.4	6.2	267.4	6.1	555.8	2706.7	8.0	658.7	12.4
MHL	247.3	647.2	7.6	293.7	6.1	539.1	2518.7	7.6	585.3	12.6
PDS	221.5	742.5	10.9	941.6	7.1	801.3	4597.4	8.5	936.1	37.3

Figure 4. Representative  $^{13}\text{C}$  NMR spectra of coal samples at various contact times: (a) HCG coal and (b) LL coal.Figure 5. Magnetization intensity of  $^{13}\text{C}$  NMR spectra at various contact times: (a) HCG, (b) XG, (c) JL, (d) LL, (e) MHL, and (f) PDS coal.

associated with the maximum intensity varies for different carbons ( $\sim 1$  ms for aliphatic carbons and typically  $> 2$  ms for aromatic carbons). Moreover, the signal of the aliphatic carbon declined more rapidly than that of the aromatic carbon after the respective peaks were reached.

As shown in Figure 6, the percentage of the aromatic region in the CP/MAS  $^{13}\text{C}$  NMR spectra increased continuously with the contact time for all coals. The aromaticity ranking among these coals was consistent, but in some cases, the contact time had an even more remarkable effect than the coal type. For example, HCG coal, which has the highest volatile matter

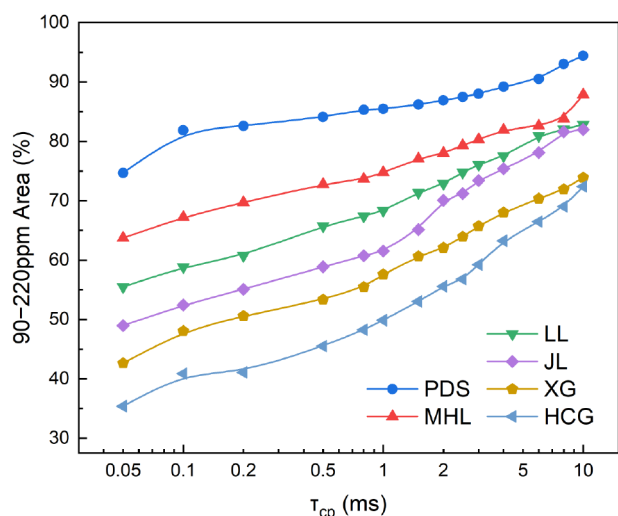


**Figure 6.** Apparent aromaticity of coal samples at various contact time.

content in this work, has an apparent aromaticity of 35% at a contact time of 0.05 ms, while it increases to 71% at 10 ms. These results suggest that quantitative tolerances may be fatal for low-rank coals if the contact time is not properly selected.

The effect of the contact time can be attributed to the different strengths of  $^1\text{H}$ – $^{13}\text{C}$  dipolar couplings for aliphatic and aromatic groups during CP experiments. Polarization rate from proton (abundant nucleus) to carbon (dilute nucleus) strongly depends on their nuclear spatial distance.<sup>34</sup> For most coal, aliphatic carbons have more directly attached hydrogen atoms compared with aromatic carbons. The distinctive aromatic skeleton structure results in a longer average distance between the aromatic carbon and the hydrogen nucleus compared to that of the aliphatic carbon in coal. At short to moderate CP contact times, the polarization for aliphatic groups is built more quickly than aromatic groups due to their stronger  $^1\text{H}$ – $^{13}\text{C}$  interaction, which may cause the underestimation of aromaticity in the  $^{13}\text{C}$  NMR spectrum. The longer contact time means more effective dipolar couplings in the aromatic skeleton. However, the CP contact time cannot be increased indefinitely due to instrument limitations and total signal attenuation. This is one of the important reasons why the CP/MAS  $^{13}\text{C}$  NMR spectrum of coal at a single contact time (with the highest signal-to-noise ratio) is typically more suitable for qualitative rather than quantitative application.

**3.2.2. CP Dynamics.** It is necessary to establish a mathematical expression for describing the CP dynamic process and the differences in polarization rates, which even makes it possible to obtain a quantitative measurement of the carbon structure in coal from variable contact time experiments. The classical method uses relaxation parameters to reflect the gross dynamics and determines carbon aromaticity by extrapolating the integrals to zero contact time.<sup>16,54,55</sup> An idealized carbon magnetization behavior is shown in Figure 7:<sup>33</sup> an exponential increase at short contact times follows a characteristic time constant  $T_{\text{CH}}$  until a state of pseudoequilibrium with the proton reservoir is achieved, and the carbon magnetization decreases at long contact times owing to the polarization of the proton reservoir during the process of spin–lattice relaxation in the rotating frame ( $T_{1\rho}^{\text{H}}$ ). As a result of

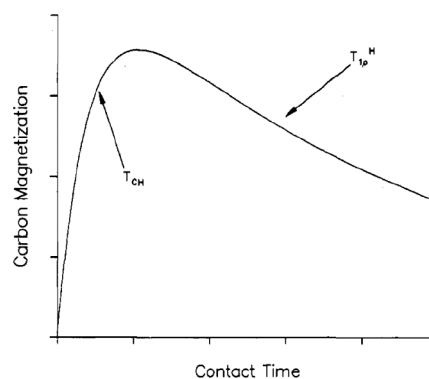


**Figure 7.** Idealized behavior of the carbon magnetization with contact time in the CP experiments (reproduced with permission from ref 33. Copyright 1987 American Chemical Society).

these two competing pathways, a successful CP/MAS  $^{13}\text{C}$  NMR spectrum must require a contact time longer than any  $T_{\text{CH}}$  to ensure that each carbon type is sufficiently polarized. Furthermore, the contact time should be shorter than any relaxation time  $T_{1\rho}^{\text{H}}$  as the carbon nuclei are in intimate contact with a polarized proton that also decays at some finite rate.<sup>33</sup>

A representative simplified exponential model containing three parameters was proposed in the 1990s to express the varying carbon magnetization with contact time, as shown in eq 2, which should be used separately for aromatic or aliphatic regions and has proven to be applicable in most cases:<sup>16</sup>

$$M(\tau_{\text{cp}}) = M_0(e^{-\tau_{\text{cp}}/T_{1\rho}^{\text{H}}} - e^{-\tau_{\text{cp}}/T_{\text{CH}}}) \quad (2)$$

where  $M_0$  is the initial magnetization intensity;  $\tau_{\text{cp}}$  is the CP contact time;  $T_{\text{CH}}$  is the polarization transfer time constant; and  $T_{1\rho}^{\text{H}}$  is the proton rotating frame spin–lattice relaxation time.

This model focuses on the overall dynamics and does not consider the different numbers of protons attached to the carbon atoms. As the polarization rate has a substantial distinction for carbon nuclei with or without bonded protons, an advanced model based on the above has been proposed to classify the magnetization into two categories, as shown in eq 3:<sup>36,56</sup>

$$\begin{aligned} M(\tau_{\text{cp}}) &= M_{\text{G}} + M_{\text{L}}, \\ M_{\text{G}} &= M_{\text{G}0}(e^{-\tau_{\text{cp}}/T_{1\rho}^{\text{H}}} - e^{-0.5(\tau_{\text{cp}}/T_{\text{GCH}})^2}), \\ M_{\text{L}} &= M_{\text{L}0}(e^{-\tau_{\text{cp}}/T_{1\rho}^{\text{H}}} - e^{-\tau_{\text{cp}}/T_{\text{LCH}}}) \end{aligned} \quad (3)$$

where  $M_{\text{G}}$  and  $M_{\text{L}}$  represent the magnetization of the polarization transfer from the bonded protons to carbon and from the unbonded protons spin diffusion, respectively;  $M_{\text{G}0}$  and  $M_{\text{L}0}$  are the initial intensities of  $M_{\text{G}}$  and  $M_{\text{L}}$ , respectively; the time constants  $T_{\text{GCH}}$  and  $T_{\text{LCH}}$  were used to describe the dynamics of the two polarization stages. This model should also be used separately for the aromatic and aliphatic regions in the CP/MAS  $^{13}\text{C}$  NMR spectra. The sum of the magnetizations for both protonated and nonprotonated carbons is indicated in eq 4, where  $(M_{\text{G}0} + M_{\text{L}0})$  represents the total magnetization in the sample with no contact time, that is, another form of  $M_0$ .

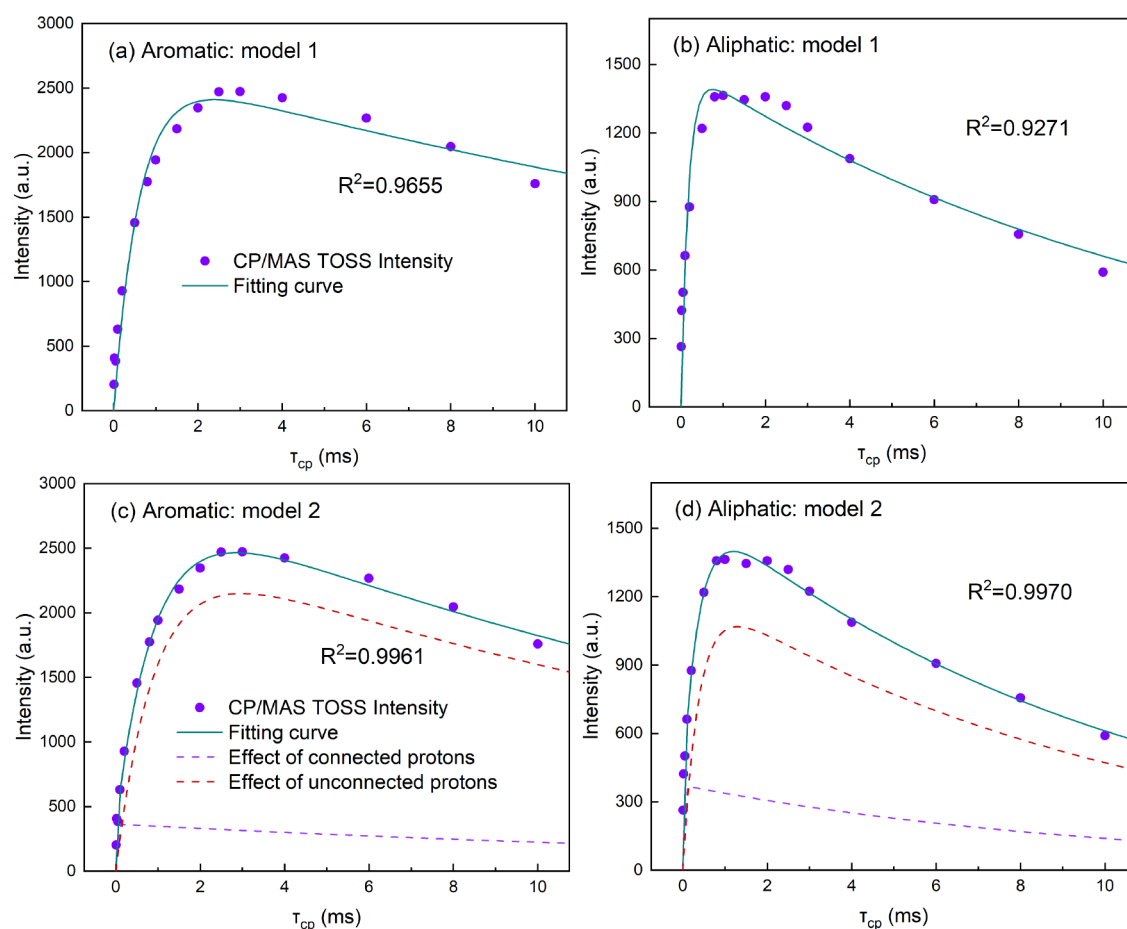


**Figure 8.** Fitting performance of CP dynamics for the magnetization intensity of XG coal: aromatic (a) and aliphatic (b) regions fitted by model 1, and aromatic (c) and aliphatic (d) regions fitted by model 2.

$$M(\tau_{cp}) = (M_{G0} + M_{L0}) e^{-\tau_{cp}/T_{1p}^H} - M_{G0} e^{-0.5(\tau_{cp}/T_{GCH})^2} - M_{L0} e^{-\tau_{cp}/T_{LCH}} \quad (4)$$

Figure 8 briefly compares the fitting curves using these two equations for the magnetization signal of XG coal, where models 1 and 2 represent the equations with one single time constant ( $T_{CH}$ ) and two time constants ( $T_{GCH}$  and  $T_{LCH}$ ), respectively. The simplified three-parameter model already correlates with the variable contact time experiments within fairly acceptable deviations. However, model 2 with more complete dynamics could perform better, particularly for the aliphatic carbon ( $R^2 > 0.996$ ). Figure 8c,d also shows the contributions of protonated and nonprotonated carbon to the total magnetization in each region, respectively, according to eq 3. The polarization transfer from unbonded proton spin diffusion accounts for the majority (>80%) and almost exclusively determines the growth in both regions. Nevertheless, the increasing rate of polarization from the protons directly connected to carbon is much faster than that from unconnected protons, and the maximum rate is achieved for a contact time of <0.1 ms. This is comparatively important for aliphatic groups containing more hydrogen and also accounts for the overestimation of aliphatic carbons by  $^{13}\text{C}$  NMR spectroscopy at short contact times.

It is not difficult to conclude from Figure 8 that the five-parameter dynamic model not only fits the total intensity more suitably but also provides more details regarding the two CP

stages. Figure S3 illustrates exhaustively all the fitting curves adopting this model for six coal samples, and the acquired dynamic parameters are listed in Table 4. A clear difference in the polarization rates between the carbons directly connected to protons or not can be observed in Table 4, as the time constant  $T_{GCH}$  (6.2–10.9  $\mu\text{s}$ ) is 2 orders of magnitude smaller than  $T_{LCH}$  and is almost independent of both carbon type and coal sample. Except for PDS anthracite with a low hydrogen content, the polarization time of the unbonded proton spin diffusion for aromatic carbons is two to three times longer than that of aliphatic carbons. Likewise, the rotating-frame spin-lattice relaxation for aromatic protons is also slower for  $T_{1p}^H$  values of 10.5–37.3 ms, compared to 6.0–10.2 ms for aliphatic protons. These time parameters reasonably describe the fact that the magnetization signal of aromatic carbons both accumulates and decays more slowly than that of aliphatic carbons. Also, this phenomenon results in a subtle counterbalance because the requirements of  $T_{CH} \ll \tau_{cp} \ll T_{1p}^H$  can hardly be fulfilled simultaneously in a single CP/MAS  $^{13}\text{C}$  NMR experiment of coal: satisfying the former is quite challenging for aromatic carbons with nearly 1 ms of  $T_{LCH}$ , while satisfying the latter requires a short contact time considering the relatively fast relaxation of aliphatic protons.

**3.3. A Potential Quantitative Modification. 3.3.1. Initial Aromaticity.** In the CP dynamic models, on the one hand, the time constants can characterize the increasing rate of magnetization signal, and on the other hand, the extrapolated

initial intensity  $M_0$  has the potential to quantify different carbon nuclei since it is ultimately a time-independent parameter derived from a series of variable contact time experiments. The more the contact times, the more accurate is the estimate of  $M_0$ . A scheme has been proposed to determine the fractions of aromatic and aliphatic carbons using initial magnetization intensity in previous studies,<sup>16,33,36,56</sup> as shown in eq 5, whereas in this work, we prefer to name them as initial aromaticity ( $f_{a0}$ ) and aliphaticity ( $f_{al0}$ ):

$$f_{a0} = \frac{M_{0a}}{M_{0a} + M_{0al}}, \quad f_{al0} = \frac{M_{0al}}{M_{0a} + M_{0al}} \quad (5)$$

where  $M_{0a}$  and  $M_{0al}$  are the initial magnetization intensities for aromatic and aliphatic carbons, respectively. For example,  $M_{0a}$  means the  $M_{G0} + M_{L0}$  value for the aromatic region of a specific coal sample in Table 4. This approach can effectively reduce the influence of the CP contact time and avoid the bias associated with the use of a single CP/MAS NMR spectrum. It is worth noting that this calculation cannot fully eliminate other factors affecting quantitative reliability, such as TOSS<sup>12</sup> and carbon invisibility due to paramagnetic centers.<sup>16,33</sup> Therefore, it can be said that eq 5 describes a hypothetical aromaticity just independent of contact time, which is why we define it as an initial aromaticity rather than a directly quantitative one.

The initial aromaticities of six coal samples are presented in Figure 9, which show a good positive correlation with the

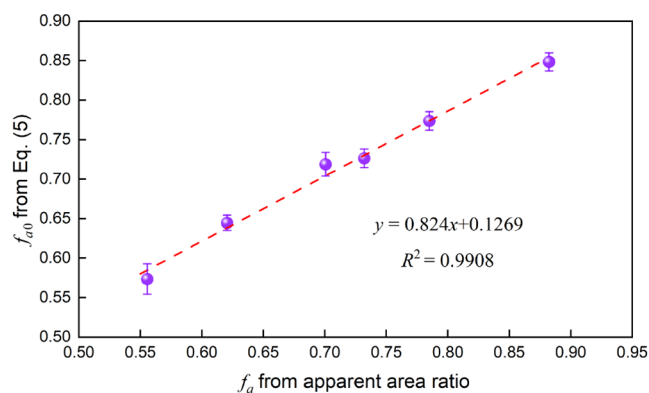


**Figure 9.** Correlation of initial and apparent aromaticities (at  $\tau_{cp} = 2$  ms).

apparent aromaticities at a standard contact time of 2 ms. A strong linear relationship can be established between them, as shown in eq 6:

$$f_{a0} = 0.824f_a + 0.1269 \quad (6)$$

which may provide a convenient approach for estimating the initial aromaticity when the conditions do not permit a sufficient period for variable contact time experiments. The correlation between the initial and apparent parameters may enable a single CP/MAS  $^{13}\text{C}$  NMR spectrum of coal potentially meaningful for quantitative applications.

**3.3.2. A Modified Calibration Method.** Standard curves are widely used for quantitative calibration in instrumental analysis. The carbon parameters of coal-like small molecules with known structures can be easily analyzed theoretically, which allows a correspondence to be developed with the apparent parameters from CP/MAS  $^{13}\text{C}$  NMR spectroscopy. A constructive method for calibration is to form the corre-

spondence of many molecules into a fitted curve, which may be helpful for determining the complex structures in coal. Chen et al.<sup>32</sup> made the first attempt using five small molecules with aromatic rings, and their fitted equation was initially validated using the molecular model of Tunlan No. 2 coal.<sup>38</sup> Subsequently, they investigated the solid-state CP/MAS  $^{13}\text{C}$  NMR spectra of 12 different coal-like model compounds and updated the regression expressions in the latest study,<sup>26</sup> as shown in eqs 7 and 8, which aimed to extend the valid range and characterize the carbon structures in coal as accurately as possible. The theoretical aromaticity showed a linear correlation with the experimental values, whereas a quadratic functional relationship was established for aliphatic carbons:

$$F_a = 32.79332 + 0.68474f_a \quad (7)$$

$$F_{al} = 4.10191 + 0.16464f_{al} + 0.0075f_{al}^2 \quad (8)$$

where  $F_a$ ,  $F_{al}$ , and  $f_a$ ,  $f_{al}$  are the theoretical and apparent experimental values (%) of the aromatic or aliphatic carbon in the coal-like compounds, respectively. The above correlations were obtained separately for the aromatic and aliphatic regions and are valid for  $7.6\% < V_{daf} < 55.6\%$ . The apparent carbon parameters of 10 coal samples were corrected by eqs 7 and 8 in their studies, and it was validated that the overestimation of aliphatic carbons by the CP/MAS  $^{13}\text{C}$  NMR spectra was effectively reduced after correction. However, in their explanations, they attributed the discrepancy between the apparent parameters and the true carbon structures to the nuclear Overhauser effect (NOE), which seemed to be misguided in some way. In fact, NOE is due to cross relaxation that occurs in direct-polarization experiments during spin-lattice relaxation in the laboratory frame.<sup>57</sup> The building up of NOE is on the scale of  $\sim 1$  s, while typical CP experiments with spin-lock applied to rigid solids are on the  $\sim 1$  ms scale.<sup>37</sup> NOE, essentially a relaxation, requires randomly fluctuating magnetic fields generated by fast large-amplitude segmental motions, which are virtually impossible to occur in coals with rigid aromatic cores at this temporal scale. Therefore, the solid-state CP/MAS  $^{13}\text{C}$  NMR spectra of coal can scarcely be influenced by NOE.

Admittedly, although the explanation does not seem convincing, this external standard calibration method is worthy of reference and is still a good attempt at quantitative characterization at the application level. There are two interesting points that deserve further discussion. First, the sum of eqs 7 and 8 may exceed 100% in some cases as the fractions of aromatic and aliphatic carbons are not normalized. Second, all experimental values were obtained at the same single contact time; in other words, the effect of contact time was not considered when the equations for the model compounds were applied to real coal. These may not cause fatal errors when the samples and test conditions are similar to those in their study. However, appropriate modifications are required to further refine this approach. The corresponding changes are as follows.

For small molecules of pure substances, it can be assumed that the characterization from the  $^{13}\text{C}$  NMR spectrum at a selected suitable contact time is sufficiently close to that from CP dynamics, whereas for the heterogeneous structures in coal, the influence of contact time is not negligible as described in the previous sections. Fortunately, the initial magnetization is independent of the contact time, and the relationship between the initial and the apparent aromaticity can be given in a

**Table 5. Modified Carbon Distribution (%) of the Coal Samples Based on Solid-State  $^{13}\text{C}$  NMR Spectra**

coal	$f_a^\#$	$f_a'$	$f_a^H$	$f_a^B$	$f_a^S$	$f_a^O$	$f_a^C$	$f_{al}^\#$	$f_{al}^3$	$f_{al}^2$	$f_{al}^1 + f_{al}^*$	$f_{al}^O$
HCG	72.84	71.45	30.19	18.67	14.68	7.91	1.39	27.16	8.15	7.79	6.38	4.85
XG	76.50	75.44	32.74	22.80	13.48	6.42	1.05	23.50	6.57	6.07	4.73	6.12
JL	81.02	80.09	34.24	24.19	14.97	6.69	0.93	18.98	5.34	5.30	4.40	3.94
LL	82.79	81.92	35.07	24.02	16.72	6.11	0.87	17.21	5.40	3.67	3.14	5.01
MHL	85.79	85.09	35.34	29.40	16.52	3.84	0.70	14.21	5.02	3.94	2.12	3.14
PDS	92.27	91.72	38.42	31.19	18.51	3.60	0.55	7.73	4.17	3.05	0.30	0.20

**Table 6. Comparison of the H/C Atomic Ratios from Ultimate Analysis and  $^{13}\text{C}$  NMR Spectra**

coal	HCG	XG	JL	LL	MHL	PDS
ultimate analysis	0.8064	0.7131	0.6680	0.6313	0.5493	0.4706
before modification	1.0122	0.8979	0.8146	0.7708	0.7306	0.6745
relative deviation (%)	25.52	25.92	21.93	22.11	33.00	43.34
after modification	0.8047	0.7377	0.6884	0.6617	0.6316	0.5937
relative deviation (%)	-0.21	3.45	3.05	4.83	14.98	26.16

simple expression, as exemplified in Figure 9 and eq 6. The introduction of initial aromaticity may deal with the shortcoming of this calibration method. A modified equation considering contact time can be obtained by replacing  $f_a$  with  $f_{a0}$  in eq 7, and expanding it yields eq 9:

$$f_a^\# = 0.3279332 + 0.68474 \times f_{a0} = 0.4148 + 0.5643f_{a0} \quad (9)$$

where  $f_a^\#$  is the modified aromaticity, and the constant in eq 7 is divided by 100 to facilitate the use of a uniform unit of 1 instead of percentage. Meanwhile, we can continue to adopt the classification proposed by Solum et al.<sup>16</sup> that the carbon in the >165 ppm region is regarded as one type of aromatic carbons, such that the fraction of aliphatic carbons ( $f_{al}^\#$ ) can be determined by the difference, no longer requiring a separate calibration:

$$f_{al}^\# = 1 - f_a^\# \quad (10)$$

The fraction of each subdivided carbon type (including carbonyl carbon) can also be treated as the total amount of aliphatic or aromatic carbon multiplied by each integral area ratio:

$$f_a^i = f_a^\# \times \frac{I_a^i}{I_{90-220}}, \quad f_{al}^i = f_{al}^\# \times \frac{I_{al}^i}{I_{0-90}} \quad (11)$$

This is based on the assumption that the entire aromatic or aliphatic region has almost the same effective spin–lattice relaxation time.<sup>16,36,37</sup> Thus, by means of eq 9–eq 11, the modified carbon structural parameters of coal can be calculated with a valid range of  $V_{daf}$  between 6% and 45%. Table 5 lists the carbon distributions of the six coal samples modified using the new calibration method. Compared with the apparent parameters in Table 3, the carbon aromaticity changes from 55%–88% to 72%–93%, and each subtype of aromatic carbon increases proportionally according to eq 11. Interestingly, the values of the modified aromaticity in Table 5 are relatively close to those obtained at 10 ms in Figure 6, which also verified that the increase in the contact time can reduce the overestimation of aliphatic carbons. However, considering the overall signal attenuation and the limitations of NMR spectrometers, it is not recommended to just extend the contact time for improving the accuracy of  $^{13}\text{C}$  NMR spectra of coal. It should be noted that the redistribution of aromatic

and aliphatic carbons does not affect their overall variation with the coal rank, as the aromatic cores always play an essential role in the stability of the carbon skeleton in coal.

**3.4. Validation and Application of the Modification Method.** **3.4.1. H/C Atomic Ratio.** This new modification method offers the opportunity for quantitative or semi-quantitative applications of a single CP/MAS  $^{13}\text{C}$  NMR spectrum of coal, given that only an additional adjustment ratio with respect to aromaticity needs to be practically calculated on the basis of the conventional peak fitting operation. The following examples mainly describe the comparisons between before and after modification and will not further focus on the carbon subtypes in the interval division and the deconvolution for the  $^{13}\text{C}$  NMR spectra of coal, which is difficult to standardize and somewhat subjective. The parameters of peak fitting (peak center, FMHW, and area) in this work are provided in Table S2 for reference. The purpose of these validations we made is to make it more convenient for other researchers to obtain  $^{13}\text{C}$  NMR spectra of coals with potentially quantitative significance instead of having to perform time-consuming experiments.

The H/C atomic ratio is a practical indicator for evaluating the accuracy of  $^{13}\text{C}$  NMR analysis. Its actual value can be considered from the ultimate analysis of coal, and it can also be deduced from the carbon structural parameters based on the  $^{13}\text{C}$  NMR spectra. Assuming that<sup>36,58</sup> approximately half of the carbon atoms bound to oxygen is attached to hydrogen and that the CH group accounts for half of  $f_{al}^1 + f_{al}^*$ , the H/C atomic ratio derived from the  $^{13}\text{C}$  NMR spectra can be estimated by eq 12:<sup>26</sup>

$$(H/C)_{\text{atom}} = f_a^H + 3f_{al}^3 + 2f_{al}^2 + (f_{al}^1 + f_{al}^*)/2 + (f_{al}^O + f_a^O)/2 + f_a^C/2 \quad (12)$$

Table 6 lists the calculation results for the six coal samples and their relative deviations before and after modification. The H/C atomic ratios of these coals ranged from 0.47 to 0.81, whereas those obtained only from spectral peak fitting ranged from 0.67 to 1.01, with an average deviation of 29%. The overestimation of the aliphatic carbon by the apparent CP/MAS  $^{13}\text{C}$  NMR spectrum leads to a higher H/C atomic ratio, as aromatic structures usually contain fewer hydrogen atoms.

The relative deviations were significantly reduced, with an average of  $\sim 20\%$  when using modified carbon parameters. The estimation yields errors of less than  $\pm 5\%$  for the first four coals. A similar trend can be identified for both before and after modification: the deviation increases as  $V_{\text{daf}}$  decreases from 44.5% to 6.6% because the approximation assumption in eq 12 may no longer be entirely applicable to high-rank coals with low hydrogen and oxygen contents. However, this does not affect the acceptability of the method in eqs 9–11, which has minimized the possible factors affecting quantification, including the CP contact time and others.

**3.4.2. FTIR Spectroscopy.** FTIR spectroscopy is another effective method for characterizing the carbon structure of coal. Generally, NMR spectroscopy focuses on the type of carbon nuclei, whereas FTIR spectroscopy mainly provides information regarding chemical bonds and functional groups. They demonstrate good agreement for some feature structures in coal,<sup>59,60</sup> and results from the FTIR spectra can be used as a contrast to reflect the objectivity of the solid-state  $^{13}\text{C}$  NMR method. Figure 10 shows the FTIR spectra of the coal samples.

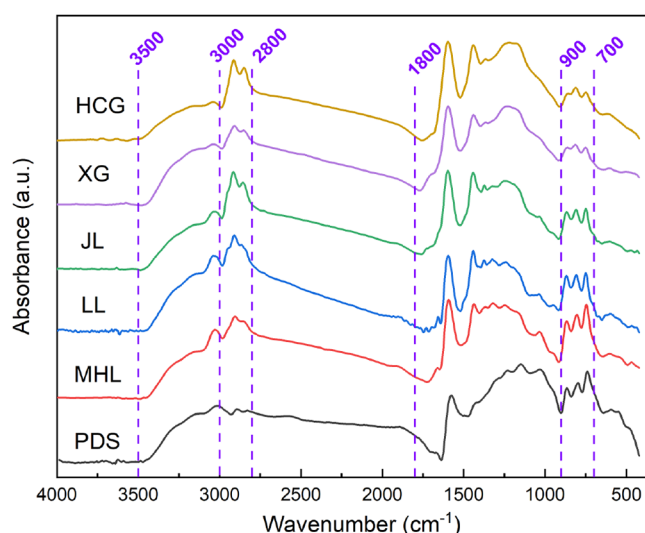


Figure 10. FTIR spectra of the coal samples.

These coals exhibited characteristic absorption bands with similar wavenumbers but different intensities. According to previous studies,<sup>38,45,53,61</sup> the FTIR spectra of coal can be divided into four regions: aromatic CH region ( $700\text{--}900\text{ cm}^{-1}$ ), oxygen functional groups region ( $1000\text{--}1800\text{ cm}^{-1}$ ), aliphatic CH region ( $2800\text{--}3000\text{ cm}^{-1}$ ), and hydroxyl region

( $3000\text{--}3600\text{ cm}^{-1}$ ). The spectra of the three carbon-containing regions were further analyzed by curve fitting to obtain the carbon structural parameters. Figure 11 shows an example of HCG coal, and the details for all coals are provided in Figure S4 and Table S3.

As shown in Figure 11, the  $700\text{--}900\text{ cm}^{-1}$  region contains aromatic C–H out-of-plane bending vibrations involving one to four adjacent H deformations.<sup>38</sup> The  $1000\text{--}1280\text{ cm}^{-1}$  spectral band is assigned to the C–O stretching vibration, and the strong intensity around  $1600\text{ cm}^{-1}$  is assigned to the aromatic skeleton C=C stretching vibrations.<sup>53</sup> The C=O stretching vibrations at  $1620\text{--}1700\text{ cm}^{-1}$  are extremely weak for all samples, which is consistent with the very small carbonyl carbon peaks in the  $^{13}\text{C}$  NMR spectra. The  $2800\text{--}3000\text{ cm}^{-1}$  region is characterized by strong aliphatic C–H stretching vibrations, mainly including the symmetric or asymmetric vibrations of  $\text{CH}_2$  and  $\text{CH}_3$  groups. The absorbance in the aromatic or aliphatic region is proportional to the concentration of C–H bonds in the same sample; thus, the proportion of aliphatic hydrogen ( $H_{\text{al}}/H$ ) can be determined using eq 13:

$$\frac{H_{\text{al}}}{H} = \frac{A_{3000-2800}}{A_{3000-2800} + A_{900-700}} \quad (13)$$

Carbon aromaticity can be obtained as shown in eq 14, given that only aromatic and aliphatic carbons are included in the carbon atoms of coal:<sup>42,45,62</sup>

$$f_a = 1 - \frac{C_{\text{al}}}{C} = 1 - \left( \frac{H_{\text{al}}}{H} \times \frac{H}{C} \right) / \frac{H_{\text{al}}}{C_{\text{al}}} \quad (14)$$

where  $H/C$  is the atomic ratio of hydrogen to carbon calculated from the ultimate analysis of coal, and  $H_{\text{al}}/C_{\text{al}}$  is the atomic ratio of hydrogen to carbon in aliphatic groups, estimated from eq 15 for different coals:<sup>60</sup>

$$H_{\text{al}}/C_{\text{al}} = -0.033 \times O_{\text{daf}} + 1.9 \quad (15)$$

The aromaticity of the coal samples calculated from the  $^{13}\text{C}$  NMR and FTIR methods is shown in Figure 12. The values obtained by either method increased with the coal rank, but the calculation based on the apparent intensity of the  $^{13}\text{C}$  NMR spectra differed remarkably from that of the FTIR method. The modification method developed in this study reduced the discrepancy to an acceptable range, with the average relative deviation decreasing from 17% to 4%. The deviations for the HCG and JL coal are less than 2%. Although the determination of aromaticity by FTIR spectroscopy has some fault tolerance as it does not involve carbonyl groups,

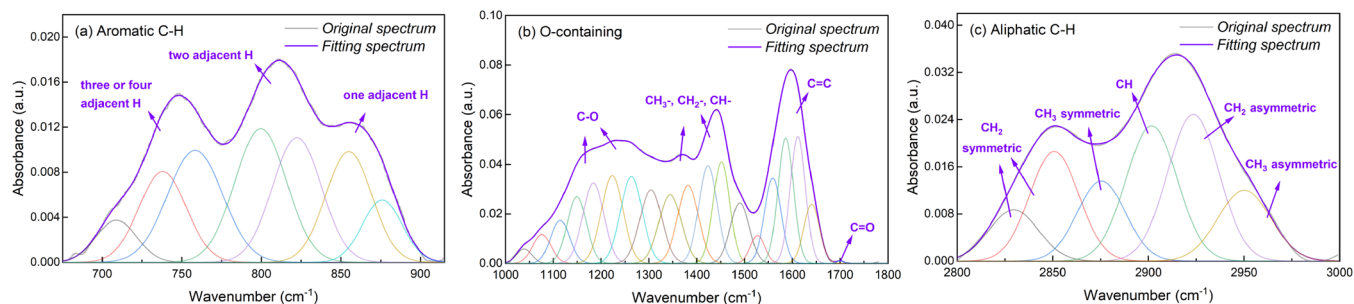
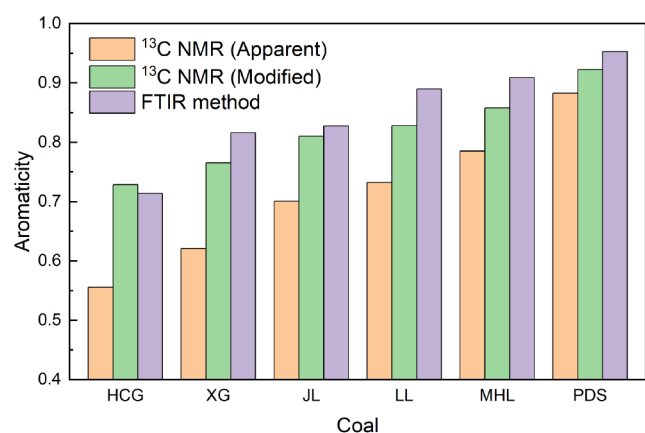


Figure 11. Fitting curve for the FTIR spectra of HCG coal: (a) aromatic CH region, (b) oxygen functional groups region, and (c) aliphatic CH region.



**Figure 12.** Comparison of aromaticity calculated from <sup>13</sup>C NMR and FTIR spectra.

and the *H/C* ratio of aliphatic groups is roughly estimated, the consistency between the <sup>13</sup>C NMR and FTIR spectroscopy is enough to validate the practicality of the modification method.

Furthermore, mutual validation of <sup>13</sup>C NMR and FTIR spectroscopy was also observed in the carbon structures of the aliphatic groups. The ratio of CH<sub>2</sub> to CH<sub>3</sub> is a valuable parameter for describing the average length of aliphatic side chains, which is related to the formation of liquid products during pyrolysis and liquefaction.<sup>25,48,53,63</sup> Figure 13 gives a

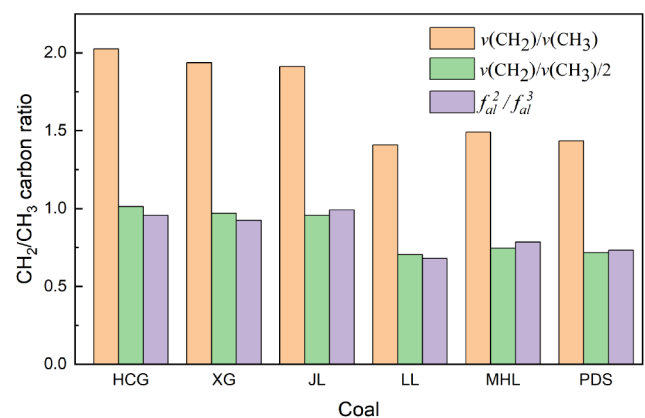


**Figure 13.** Comparison of CH<sub>2</sub>/CH<sub>3</sub> in carbon structures of coal from <sup>13</sup>C NMR and FTIR spectra.

comparison of the calculation results obtained by using different approaches. The carbon parameters from the <sup>13</sup>C NMR spectra directly reflect the number of carbon atoms, whereas the vibrational intensity in the FTIR spectra provides a measurement of the chemical bonds in the entire group. The carbon atom number ratio  $f_{al}^2/f_{al}^3$  is in excellent agreement with the absorbance ratio of CH<sub>2</sub> to CH<sub>3</sub> divided by two for all coal samples, which may result from that the number of C–H bond stretching vibration types for each CH<sub>2</sub> group is half that of the CH<sub>3</sub> group. The difference is less than 0.05 for each sample. Coals with low *V*<sub>daf</sub> values (such as LL, MHL, and PDS) had

smaller CH<sub>2</sub>/CH<sub>3</sub> ratios, representing a lower branching degree and relatively compact carbon structures, which means it is more difficult to form liquid products with moderate molecular weight during the thermal conversion process.

**3.4.3. Aromaticity Correlations.** Additionally, the aromaticity of coal can be predicted by empirical correlations associated with the elemental compositions. They have acceptable accuracy and have been widely applied to estimate the carbon structures of coal, char, and tar.<sup>46,47</sup> The earliest aromaticity correlation was established by Van Krevelen et al.<sup>64,65</sup> with respect to the volatile matter and carbon content of coal, as shown in eq 16:

$$f_a = (100 - V_{daf}) \times 1200 / (1240 \times C_{daf}) \quad (16)$$

A linear correlation based on the carbon content was proposed by Niksa et al.,<sup>21–23</sup> as shown in eq 17. It was adopted in the coal pyrolysis FLASHCHAIN model that they developed, which used <sup>13</sup>C NMR parameters to identify the coal structure and simplified the mechanism of bridge cleavage devolatilization to predict the pyrolysis yields of tar, char, and gas.

$$f_a = 0.0159 \times C_{daf} - 0.564 \quad (17)$$

Maroto-Valer et al.<sup>66,67</sup> conducted single-pulse excitation <sup>13</sup>C NMR experiments on more than 30 different coals and correlated the derived aromaticity with the *H/C* atomic ratio for bituminous coals, as shown in eq 18. Mazumdar<sup>68</sup> further discussed the applicable conditions and required adjustments related to the coal rank.

$$f_a = 1.22 - 0.58 \times (H/C)_{atom} \quad (18)$$

A general correlation with nine coefficients was developed by Richards et al.<sup>46</sup> based on a large collection of data from the literature and a comparison of several existing models, as shown in eq 19. This formula has the same form as the chemical structure parameters of the CPD coal pyrolysis model.<sup>69</sup> They used the strict aromaticity ( $f'_a$ ) excluding carbonyl groups. The coefficients are listed in Table 7; and the carbon, hydrogen, oxygen, and volatile matter contents were all on a dry and ash-free basis.

$$f'_a = c_1 + c_2C + c_3C^2 + c_4H + c_5H^2 + c_6O + c_7O^2 + c_8V + c_9V^2 \quad (19)$$

The aromaticity of the coal samples in this study has also been calculated using these empirical formulas, according to the proximate and ultimate analyses in Table 1. The calculation values were compared with the aromaticity derived from the apparent and modified CP/MAS <sup>13</sup>C NMR experimental results, as shown in Figure 14. It can be evidently seen from Figure 14a that all the predicted values are much higher than the apparent aromaticity obtained from <sup>13</sup>C NMR spectra, which is consistent with the previous discussion. After modification using eq 9, the overestimation of the aromatic carbon improved. The deviations between modified aromaticity and the prediction of these empirical correlations were

**Table 7.** Coefficients of Aromaticity Correlation

<i>c</i> <sub>1</sub>	<i>c</i> <sub>2</sub>	<i>c</i> <sub>3</sub>	<i>c</i> <sub>4</sub>	<i>c</i> <sub>5</sub>	<i>c</i> <sub>6</sub>	<i>c</i> <sub>7</sub>	<i>c</i> <sub>8</sub>	<i>c</i> <sub>9</sub>
4.384	−8.679 × 10 <sup>−2</sup>	5.352 × 10 <sup>−4</sup>	2.601 × 10 <sup>−2</sup>	−6.879 × 10 <sup>−3</sup>	3.525 × 10 <sup>−3</sup>	−5.710 × 10 <sup>−4</sup>	−2.666 × 10 <sup>−3</sup>	5.659 × 10 <sup>−6</sup>

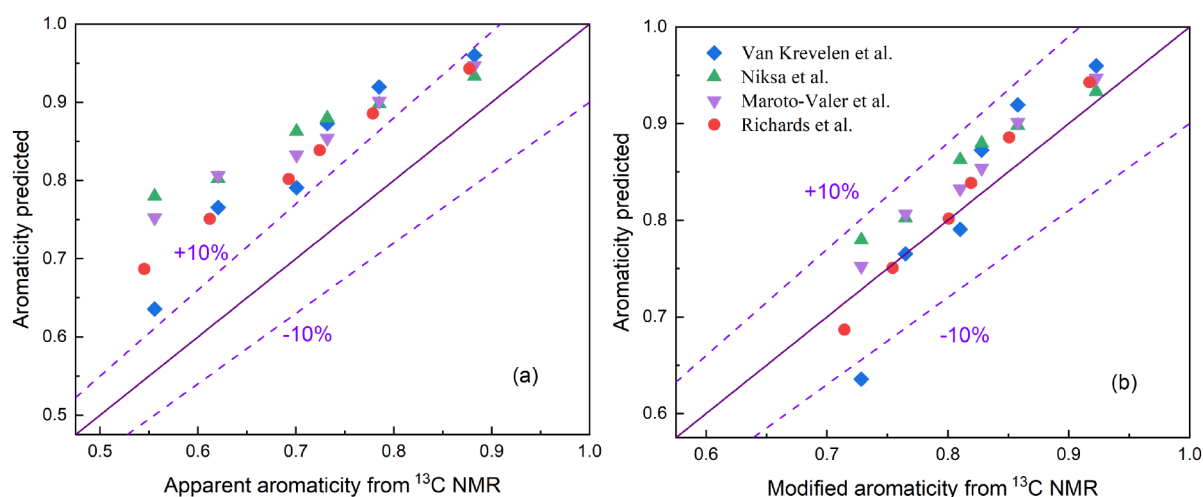


**Figure 14.** Comparison of aromaticity between different correlations and  $^{13}\text{C}$  NMR spectral methods: (a) apparent and (b) modified values.

significantly reduced, almost always within  $\pm 10\%$ , as shown in Figure 14b. The smallest deviation was obtained using the formula proposed by Richards et al.,<sup>46</sup> with an average deviation of only 2%. A probable reason for this is that their correlation was built on a considerable amount of published data and therefore had the widest applicability. This good agreement also indicates the validity and necessity of our proposed modification for the CP/MAS  $^{13}\text{C}$  NMR spectra of coal.

#### 4. CONCLUSIONS

The solid-state  $^{13}\text{C}$  NMR spectroscopy can characterize the carbon structure of coal. In this study, a series of CP/MAS experiments were conducted using coals with six different  $V_{\text{daf}}$  values. The effect of contact time was analyzed using representative dynamics models, and a modification method based on initial magnetization was proposed to quantify the carbon distribution in coal. The main conclusions are as follows:

(1) Experimental results at variable contact times from 0.01 to 10 ms indicated that the aromatic and aliphatic carbons have different efficiencies of cross-polarization. The nonprotonated carbon of the aromatic groups was polarized two to three times more slowly than that of the aliphatic groups. The apparent aromaticity increased with the contact time for all coal samples. It is not easy for a single CP/MAS  $^{13}\text{C}$  NMR experiment to ensure that each type of carbon is sufficiently polarized before the signal decay of the proton spin–lattice relaxation.

(2) The initial magnetization intensities independent of contact time were obtained using a classical five-parameter model for CP dynamics. A good linear correlation was established between the apparent and initial aromaticity, which was introduced into an existing calibration method to refine the effect of contact time. Modified carbon structural parameters of the coal samples were calculated through the redistribution of aromatic and aliphatic carbons.

(3) It was validated that the modification method showed better agreement in terms of the  $H/C$  atomic ratio of coal, FTIR spectroscopy, and empirical aromaticity correlations. These results will make the typical CP/MAS  $^{13}\text{C}$  NMR spectra of coal have the potential to be quantitatively meaningful at the application level.

#### ASSOCIATED CONTENT

##### Supporting Information

The Supporting Information is available free of charge at <https://pubs.acs.org/doi/10.1021/acs.energyfuels.3c04714>.

Pre-experimental results and detailed illustration of fitting curves for the  $^{13}\text{C}$  NMR and FTIR spectra of all coal samples, Figures S1–S5 and Tables S1–S4 (PDF) Peak parameters of the fitting curves for the  $^{13}\text{C}$  NMR and FTIR spectra, Tables S2 and S3 (XLSX)

#### AUTHOR INFORMATION

##### Corresponding Author

Mengxiang Fang – State Key Laboratory of Clean Energy Utilization, Zhejiang University, Hangzhou 310027, PR China; Qingshanhu Energy Research Center, Zhejiang University, Hangzhou 311300, PR China; [orcid.org/0000-0002-3282-8756](https://orcid.org/0000-0002-3282-8756); Email: [mxfang@zju.edu.cn](mailto:mxfang@zju.edu.cn)

##### Authors

Tong Lv – State Key Laboratory of Clean Energy Utilization, Zhejiang University, Hangzhou 310027, PR China; Qingshanhu Energy Research Center, Zhejiang University, Hangzhou 311300, PR China; [orcid.org/0000-0002-3252-7486](https://orcid.org/0000-0002-3252-7486)

Xi Zeng – State Key Laboratory of Clean Energy Utilization, Zhejiang University, Hangzhou 310027, PR China; College of Electrical Engineering, Guizhou University, Guiyang 550025, PR China

Jiqing Yan – State Key Laboratory of Clean Energy Utilization, Zhejiang University, Hangzhou 310027, PR China

Yu Huang – State Key Laboratory of Clean Energy Utilization, Zhejiang University, Hangzhou 310027, PR China

Jianmeng Cen – State Key Laboratory of Clean Energy Utilization, Zhejiang University, Hangzhou 310027, PR China; Qingshanhu Energy Research Center, Zhejiang University, Hangzhou 311300, PR China

Qinhui Wang – State Key Laboratory of Clean Energy Utilization, Zhejiang University, Hangzhou 310027, PR China; Qingshanhu Energy Research Center, Zhejiang University, Hangzhou 311300, PR China; [orcid.org/0000-0002-5190-6932](https://orcid.org/0000-0002-5190-6932)

Complete contact information is available at:  
<https://pubs.acs.org/10.1021/acs.energyfuels.3c04714>

## Notes

The authors declare no competing financial interest.

## ACKNOWLEDGMENTS

This work was supported by the National Natural Science Foundation of China (No. U1910201) and the Fundamental Research Funds for the Central Universities (No. 2022ZFJH04).

## NOMENCLATURE

$A$	area; ash content
$f_a$	aromaticity
$f_{a0}$	initial aromaticity
$f_a^\#$	modified aromaticity
$f_a'$	fraction of carbon in aromatic rings
$f_a^B$	fraction of bridgehead aromatic carbons
$f_a^C$	fraction of carbon in carboxyl or carbonyl
$f_a^H$	fraction of protonated aromatic carbons
$f_a^O$	fraction of aromatic carbons bonded to oxygen
$f_a^S$	fraction of alkylated aromatic carbons
$f_{al}$	aliphaticity
$f_{al0}$	initial aliphaticity
$f_{al}^\#$	modified aliphaticity
$f_{al}^3$	fraction of aliphatic carbons in methyl
$f_{al}^2$	fraction of aliphatic carbons in methylene
$f_{al}^1$	fraction of aliphatic carbons in methine
$f_{al}^*$	fraction of aliphatic quaternary carbons
$f_{al}^O$	fraction of aliphatic carbons bonded to oxygen
$F_a$	fraction of aromatic carbons in model compounds
$F_{al}$	fraction of aliphatic carbons in model compounds
$I$	intensity
$M_0$	initial magnetization
$M_G$	magnetization of polarization transfer from bonded protons to carbon
$M_{G0}$	initial intensity of $M_G$
$M_L$	magnetization of polarization transfer from unbonded protons spin diffusion
$M_{L0}$	initial intensity of $M_L$
$T_{CH}$	polarization transfer time constant, $\mu s$
$T_{GCH}$	polarization transfer time constant from bonded protons to carbon, $\mu s$
$T_{LCH}$	polarization transfer time constant from unbonded protons spin diffusion, $\mu s$
$T_{1\rho}^H$	proton rotating frame spin–lattice relaxation time, ms
$\nu$	vibration
$V$	volatile matter
$\tau_{cp}$	cross-polarization contact time, ms
$\delta$	chemical shift, ppm

## Subscript

a aromatic  
 al aliphatic

## Acronyms

AW acid washed  
 CP cross-polarization  
 CPD chemical percolation devolatilization

FC fixed carbon  
 FTIR Fourier transform infrared  
 MAS magic angle spinning  
 NMR nuclear magnetic resonance  
 NOE nuclear Overhauser effect  
 BMCP Boltzmann–Monte Carlo percolation  
 TOSS total suppression of spinning sidebands

## REFERENCES

- (1) Yu, P.; Luo, Z.; Wang, Q.; Fang, M. Life cycle assessment of transformation from a sub-critical power plant into a polygeneration plant. *Energy Convers. Manage.* **2019**, *198*, 111801.
- (2) Lv, T.; Fang, M.; Li, H.; Yan, J.; Cen, J.; Xia, Z.; Tian, J.; Wang, Q. Pyrolysis of a typical low-rank coal: Application and modification of the chemical percolation devolatilization model. *R.S.C. Adv.* **2021**, *11* (29), 17993–18002.
- (3) Lv, J.; Wang, G.; Jin, L.; Wang, D.; Li, Y.; Hu, H. Process parameter optimization for integrated process of coal pyrolysis with dry reforming of low carbon alkane over Ni/La<sub>2</sub>O<sub>3</sub>–ZrO<sub>2</sub>. *J. Energy. Inst.* **2022**, *102*, 54–59.
- (4) Guo, Z.; Wang, Q.; Fang, M.; Luo, Z.; Cen, K. Thermodynamic and economic analysis of polygeneration system integrating atmospheric pressure coal pyrolysis technology with circulating fluidized bed power plant. *Appl. Energy* **2014**, *113*, 1301–1314.
- (5) Wang, D.; Jin, L.; Wei, B.; Lv, J.; Li, Y.; Hu, H. Oxidative catalytic cracking and reforming of coal pyrolysis volatiles over NiO. *Energy Fuels* **2020**, *34* (6), 6928–6937.
- (6) Lei, Z.; Cheng, Z.; Ling, Q.; Liu, X.; Cui, P.; Zhao, Z. Investigating the trigger mechanism of Shenfu bituminous coal pyrolysis. *Fuel* **2022**, *313*, 122995.
- (7) Qin, X.; Yang, T.; Liu, Z.; Liu, Q. Molecular structure, bond cleavage and their relation of four low rank coals. *Fuel Process. Technol.* **2022**, *236*, 107391.
- (8) Lin, D.; Liu, L.; Zhao, Y.; Zhao, Y.; Qiu, P.; Xie, X.; Sun, S. Influence of pyrolysis pressure on structure and combustion reactivity of Zhundong demineralized coal char. *J. Energy. Inst.* **2020**, *93* (5), 1798–1808.
- (9) Yan, L.; Wang, W.; Liu, Y.; Wang, M.; Li, F.; Bao, W. The roles of low molecular compounds on the light aromatics formation during different rank coal pyrolysis. *J. Energy. Inst.* **2022**, *100*, 129–136.
- (10) Suggate, R. P.; Dickinson, W. W. Carbon NMR of coals: the effects of coal type and rank. *Int. J. Coal Geol.* **2004**, *57* (1), 1–22.
- (11) Solum, M. S.; Sarofim, A. F.; Pugmire, R. J.; Fletcher, T. H.; Zhang, H. <sup>13</sup>C NMR analysis of soot produced from model compounds and a coal. *Energy Fuels* **2001**, *15* (4), 961–971.
- (12) Snape, C. E.; Axelson, D. E.; Botto, R. E.; Delpuech, J. J.; Tekely, P.; Gerstein, B. C.; Pruski, M.; Maciel, G. E.; Wilson, M. A. Quantitative reliability of aromaticity and related measurements on coals by <sup>13</sup>C n.m.r. A debate. *Fuel* **1989**, *68* (5), 547–548.
- (13) Qian, L.; Tao, C.; Ma, C.; Xue, J.; Guo, F.; Jia, X.; Yan, W. Construction of a macromolecular structure model for Zhundong subbituminous coal. *J. Mol. Struct.* **2022**, *1248*, 131496.
- (14) Xu, F.; Pan, S.; Liu, C.; Zhao, D.; Liu, H.; Wang, Q.; Liu, Y. Construction and evaluation of chemical structure model of Huolinhe lignite using molecular modeling. *R.S.C. Adv.* **2017**, *7* (66), 41512–41519.
- (15) Lin, X.; Luo, M.; Li, S.; Yang, Y.; Chen, X.; Tian, B.; Wang, Y. The evolutionary route of coal matrix during integrated cascade pyrolysis of a typical low-rank coal. *Appl. Energy* **2017**, *199*, 335–346.
- (16) Solum, M. S.; Pugmire, R. J.; Grant, D. M. Carbon-13 solid-state NMR of Argonne-premium coals. *Energy Fuels* **1989**, *3* (2), 187–193.
- (17) Zhang, P.; Li, L.; Ye, C. Solid state <sup>13</sup>C NMR study of Chinese coals. *Fuel Sci. Technol. Int.* **1995**, *13* (4), 467–481.
- (18) Yao, Q.; Ma, M.; Liu, Y.; Ma, D.; Chen, H.; Hao, Q.; Sun, M.; Ma, X. The structural and pyrolysis characteristics of vitrinite and inertinite from Shendong coal and the gasification performance of chars. *J. Anal. Appl. Pyrolysis* **2022**, *164*, 105519.

- (19) Grant, D. M.; Pugmire, R. J.; Fletcher, T. H.; Kerstein, A. R. Chemical model of coal devolatilization using percolation lattice statistics. *Energy Fuels* **1989**, *3* (2), 175–186.
- (20) Fletcher, T. H.; Kerstein, A. R.; Pugmire, R. J.; Solum, M. S.; Grant, D. M. Chemical percolation model for devolatilization. 3. Direct use of carbon-13 NMR data to predict effects of coal type. *Energy Fuels* **1992**, *6* (4), 414–431.
- (21) Niksa, S.; Kerstein, A. R. FLASHCHAIN theory for rapid coal devolatilization kinetics. 1. Formulation. *Energy Fuels* **1991**, *5* (5), 647–665.
- (22) Niksa, S. FLASHCHAIN theory for rapid coal devolatilization kinetics. 2. Impact of operating conditions. *Energy Fuels* **1991**, *5* (5), 665–673.
- (23) Niksa, S. FLASHCHAIN theory for rapid coal devolatilization kinetics. 3. Modeling the behavior of various coals. *Energy Fuels* **1991**, *5* (5), 673–683.
- (24) Liu, P.; Zhang, D. Effect of hydrothermal treatment on the carbon structure of Inner Mongolia lignite. *Int. J. Coal Sci. Technol.* **2020**, *7* (3), 493–503.
- (25) Liu, P.; Le, J.; Wang, L.; Pan, T.; Lu, X.; Zhang, D. Relevance of carbon structure to formation of tar and liquid alkane during coal pyrolysis. *Appl. Energy* **2016**, *183*, 470–477.
- (26) Liu, P.; Zhang, Y.; Pan, T.; Zhang, D.; Chen, L.; Sun, C. Accurately quantifying carbon structural types and predicting pyrolysis behavior of coal using solid <sup>13</sup>C NMR Cp/MAS spectra. *Fuel* **2022**, *327*, 125092.
- (27) Zhang, D.; Liu, P.; Lu, X.; Wang, L.; Pan, T. Upgrading of low rank coal by hydrothermal treatment: Coal tar yield during pyrolysis. *Fuel Process. Technol.* **2016**, *141*, 117–122.
- (28) Yoshida, T.; Sasaki, M.; Ikeda, K.; Mochizuki, M.; Nogami, Y.; Inokuchi, K. Prediction of coal liquefaction reactivity by solid state <sup>13</sup>C NMR spectral data. *Fuel* **2002**, *81* (11–12), 1533–1539.
- (29) Wei, Z.; Baiquan, L.; Tong, L. Construction of Pingdingshan coal molecular model based on FT-IR and <sup>13</sup>C-NMR. *J. Mol. Struct.* **2022**, *1262*, 132992.
- (30) Yan, J.; Jiao, H.; Li, Z.; Lei, Z.; Wang, Z.; Ren, S.; Shui, H.; Kang, S.; Yan, H.; Pan, C. Kinetic analysis and modeling of coal pyrolysis with model-free methods. *Fuel* **2019**, *241*, 382–391.
- (31) Wang, X.; Dong, Z.; Yu, R. Creation and generation mechanism of macromolecular representation for dongsheng coal vitrinite. *ACS Omega* **2022**, *7* (13), 11033–11043.
- (32) Chen, L.; Wang, L.; Pan, T.; Zhou, Y.; Zhang, Y.; Zhang, D. Calibration of solid state NMR carbon structural parameters and application in coal structure analysis. *J. Fuel Chem. Technol.* **2017**, *45* (10), 1153–1163.
- (33) Botto, R. E.; Wilson, R.; Winans, R. E. Evaluation of the reliability of solid <sup>13</sup>C-NMR spectroscopy for the quantitative analysis of coals: Study of whole coals and maceral concentrates. *Energy Fuels* **1987**, *1* (2), 173–181.
- (34) Law, R. V.; Sherrington, D. C.; Snape, C. E. Quantitative solid state <sup>13</sup>C NMR studies of highly cross-linked poly(divinylbenzene) resins. *Macromolecules* **1997**, *30* (10), 2868–2875.
- (35) Li, H.; Liang, S.; Hou, Y.; Wang, Y.; Ren, S.; Wu, W. A study on the structure of Naomaohu coal and its suitability for direct coal liquefaction. *Fuel Process. Technol.* **2022**, *227*, 107135.
- (36) Yang, H.; Xiong, Y.; Xie, Z.; Jin, L.; Li, Y.; Yang, J.; Hu, H. Quantitative characterization of coal structure by high-resolution CP/MAS <sup>13</sup>C solid-state NMR spectroscopy. *Proc. Combust. Inst.* **2021**, *38* (3), 4161–4170.
- (37) Guo, X.; Shi, L.; Liu, Z.; Xu, X.; Liu, Q.; Xue, X.; Li, X. The Boltzmann-Monte-Carlo-Percolation (BMCP) model on pyrolysis of coal: The quantitative correction on CP/MAS <sup>13</sup>C solid-state NMR spectra and insight on structural evolution during coalification. *Fuel* **2021**, *304*, 121488.
- (38) Bian, J.; Li, X.; Zeng, F.; Wang, X. Construction and evaluation of a medium-rank coal molecular model using a hybrid experimental–simulation–theoretical method. *Energy Fuels* **2019**, *33* (12), 12905–12915.
- (39) Lin, B.; Zha, W.; Liu, T. Experimental study on molecular structure differences between the tectonic coal and primary coal in Pingdingshan coalfield. *Vib. Spectrosc.* **2019**, *103*, 102930.
- (40) Ping, A.; Xia, W.; Peng, Y.; Xie, G. Construction of bituminous coal vitrinite and inertinite molecular assisted by <sup>13</sup>C NMR, FTIR and XPS. *J. Mol. Struct.* **2020**, *1222*, 128959.
- (41) Jia, J.; Wu, Y.; Zhao, D.; Li, B.; Wang, D.; Wang, F.; Chen, Y. Molecular structure characterization analysis and molecular model construction of anthracite. *PLoS One* **2022**, *17* (9), No. e0275108.
- (42) Chen, X.; Li, M.; Zeng, F. Control of chemical structure on the characteristics of micropore structure in medium-rank coals. *Fuel Process. Technol.* **2022**, *228*, 107162.
- (43) Wang, Q.; Li, K.; Guo, Z.; Fang, M.; Luo, Z.; Cen, K. Effects of CO<sub>2</sub> atmosphere on slow pyrolysis of high-ash lignite. *Carbon Resour. Convers.* **2018**, *1* (1), 94–103.
- (44) Ibarra, J. V.; Munoz, E.; Moliner, R. FTIR study of the evolution of coal structure during the coalification process. *Org. Geochem.* **1996**, *24* (6–7), 725–735.
- (45) He, X.; Liu, X.; Nie, B.; Song, D. FTIR and Raman spectroscopy characterization of functional groups in various rank coals. *Fuel* **2017**, *206*, 555–563.
- (46) Richards, A. P.; Johnson, C.; Fletcher, T. H. Correlations of the Elemental Compositions of Primary Coal Tar and Char. *Energy Fuels* **2019**, *33* (10), 9520–9537.
- (47) Mathews, J. P.; Krishnamoorthy, V.; Louw, E.; Tchapda, A. H. N.; Castro-Marciano, F.; Karri, V.; Alexis, D. A.; Mitchell, G. D. A review of the correlations of coal properties with elemental composition. *Fuel Process. Technol.* **2014**, *121*, 104–113.
- (48) Liu, P.; Zhang, D.; Wang, L.; Zhou, Y.; Pan, T.; Lu, X. The structure and pyrolysis product distribution of lignite from different sedimentary environment. *Appl. Energy* **2016**, *163*, 254–262.
- (49) Chen, S.; Zhou, W.; Ding, Y.; Zhao, G.; Gao, J. Coal-assisted water electrolysis for hydrogen production: Evolution of carbon structure in different-rank coal. *Energy Fuels* **2021**, *35* (4), 3512–3520.
- (50) Hao, P.; Meng, Y.; Zeng, F.; Yan, T.; Xu, G. Quantitative study of chemical structures of different rank coals based on infrared spectroscopy. *Spectrosc. Spectr. Anal.* **2020**, *40* (3), 787–792.
- (51) Wang, S.; Tang, Y.; Schobert, H. H.; Guo, Y. N.; Su, Y. FTIR and <sup>13</sup>C NMR investigation of coal component of late permian coals from southern China. *Energy Fuels* **2011**, *25* (12), 5672–5677.
- (52) Bertarello, A.; Berruyer, P.; Skantze, U.; Sardana, S.; Sardana, M.; Elmore, C. S.; Schade, M.; Chiarparin, E.; Schantz, S.; Emsley, L. Quantification of magic angle spinning dynamic nuclear polarization NMR spectra. *J. Magn. Reson.* **2021**, *329*, 107030.
- (53) Gao, B.; Wu, C.; Song, Y.; Zhou, D.; Niu, Q.; Zhou, H.; Jiang, X. Structural characterization of high fidelity for bituminous and semi-anthracite: Insights from spectral analysis and modeling. *Fuel* **2022**, *315*, 123183.
- (54) Abelmann, K.; Totsche, K. U.; Knicker, H.; Kögel-Knabner, I. CP dynamics of heterogeneous organic material: characterization of molecular domains in coals. *Solid State Nucl. Magn. Reson.* **2004**, *25* (4), 252–266.
- (55) Mallard, I.; Baudalet, D.; Castiglione, F.; Ferro, M.; Panzeri, W.; Ragg, E.; Mele, A. Polydisperse methyl  $\beta$ -cyclodextrin–epichlorohydrin polymers: variable contact time <sup>13</sup>C CP-MAS solid-state NMR characterization. *Beilstein. J. Org. Chem.* **2015**, *11*, 2785–2794.
- (56) Pugmire, R. J.; Solum, M. S.; Grant, D. M.; Critchfield, S.; Fletcher, T. H. Structural evolution of matched tar-char pairs in rapid pyrolysis experiments. *Fuel* **1991**, *70* (3), 414–423.
- (57) Zhang, R.; Mroue, K. H.; Ramamoorthy, A. Hybridizing cross-polarization with NOE or refocused-INEPT enhances the sensitivity of MAS NMR spectroscopy. *J. Magn. Reson.* **2016**, *266*, 59–66.
- (58) Bailey, N. T.; Ikejani, A. O. O.; Lawson, G. J.; Monsef-Mirzai, P. Measurement of hydroxyl groups in coals of different rank by acetylation with ketene and other reagents. *Fuel* **1992**, *71* (1), 45–52.

- (59) Ibarra, J.; Cervero, I.; Miranda, J.; Moliner, R. Structural rank parameters of Spanish low rank coals and their influence on pyrolysis yields. *Fuel Process. Technol.* **1991**, *28* (3), 259–273.
- (60) Dela Rosa, L.; Pruski, M.; Lang, D.; Gerstein, B.; Solomon, P. Characterization of the Argonne premium coals by using hydrogen-1 and carbon-13 NMR and FT-IR spectroscopies. *Energy Fuels* **1992**, *6* (4), 460–468.
- (61) Lin, H.; Wang, Y.; Gao, S.; Xue, Y.; Yan, C.; Han, S. Chemical structural characteristics of high inertinite coal. *Fuel* **2021**, *286*, 119283.
- (62) Ibarra, J. V.; Moliner, R.; Bonet, A. J. FT-i.r. investigation on char formation during the early stages of coal pyrolysis. *Fuel* **1994**, *73* (6), 918–924.
- (63) Song, Y.; Jiang, B.; Mathews, J. P.; Yan, G.; Li, F. Structural transformations and hydrocarbon generation of low-rank coal (vitrinite) during slow heating pyrolysis. *Fuel Process. Technol.* **2017**, *167*, 535–544.
- (64) Van Krevelen, D. W.. *Coal*; Elsevier scientific publishing company: Amsterdam, 1961.
- (65) Yan, J.; Lei, Z.; Li, Z.; Wang, Z.; Ren, S.; Kang, S.; Wang, X.; Shui, H. Molecular structure characterization of low-medium rank coals via XRD, solid state  $^{13}\text{C}$  NMR and FTIR spectroscopy. *Fuel* **2020**, *268*, 117038.
- (66) Maroto-Valer, M. M.; Love, G. D.; Snape, C. E. Relationship between carbon aromaticities and HC ratios for bituminous coals. *Fuel* **1994**, *73* (12), 1926–1928.
- (67) Maroto-Valer, M. M.; Andresen, J. M.; Snape, C. E. Verification of the linear relationship between carbon aromaticities and H/C ratios for bituminous coals. *Fuel* **1998**, *77* (7), 783–785.
- (68) Mazumdar, B. K. On the relationship between carbon aromaticities and H/C ratios for bituminous coals. *Fuel* **1999**, *78* (10), 1239–1241.
- (69) Genetti, D.; Fletcher, T. H.; Pugmire, R. J. Development and application of a correlation of  $^{13}\text{C}$  NMR chemical structural analyses of coal based on elemental composition and volatile matter content. *Energy Fuels* **1999**, *13* (1), 60–68.